Inverse Estimation of the Wall Temperature in Stagnation Region of Impinging Flow on the Cylinder with Uniform Transpiration

Mohammadiun, Mohammad*[*+]*; Mohammadiun, Hamid;
Montazeri, Mostafa; Momeni, Arsalan; Dibaee Bonab, Mohammad Hossein
Department of Mechanical Engineering, Shahrood Branch, Islamic Azad University, Shahrood, I. R. IRAN

Vahidifar, Saeed
Department of Mechanical Engineering, Technical and Vocational University (TVU), Mashhad, I. R. IRAN

Mihani, Sahebeh
Department of Civil Engineering, Shahrood Branch, Islamic Azad University, Shahrood, I. R. IRAN

Naeimabadi, Mehdi
Department of Mechanical Engineering, Shahrood Branch, Islamic Azad University, Shahrood, I. R. IRAN

ABSTRACT: *In this paper, for the first time, a numerical code based on the Levenberg–Marquardt method is presented to solve the inverse heat transfer problem of an annular jet on a cylinder with uniform transpiration and estimate the time-dependent wall temperature using temperature distribution at a point. Also, the effect of noisy data on the final result is studied. For this purpose, the immediate task is to solve the temperature with no dimensions and convection Heat transfer in a cylinder with a radial incompressible flow numerically. The free stream is steady, and the initial strain rate of flow is* $\bar{k}$*. The equations of momentum and energy are transformed into semi-similar equations using similarity variables. After discretizing the new equation system using the finite difference technique, it is solved by using the tri-diagonal matrix algorithm. After that, the wall temperature is calculated throughout using the Levenberg–Marquardt approach. This is a collaborative technique aimed at minimizing the least-square summation of the error values, where the error indicates the difference between the predicted and observed temperatures. This method exhibits considerable stability for noisy input data. In most cases, surface blowing decreases the prediction accuracy by displacement of the boundary layers from the surface, whereas suction acts vice versa. The main reason for this study is that in many industrial applications, it is not possible to insert the sensor on the wall to measure the temperature of the wall the sensor can be inserted in another place and the wall temperature distribution can be obtained by inverse analysis (Determining of unknown boundary condition).*

KEYWORDS: *Inverse heat transfer; Annular jet; Finite difference method; Momentum and energy equations; Levenberg–Marquardt method; Noisy input data.*

**To whom correspondence should be addressed.*
+ E-mail: mmohammadiun@iau-shahrood.ac.ir
1021-9986/2023/9/3083-3101 19/$/6.09

INTRODUCTION

The direct heat transfer issue is concerned with finding the temperature of interior locations inside an area given at the beginning and boundary circumstances, along with thermo physical properties such as heat production, heat flow, or temperature [1].

Inverse heat transfer problems, in contrast, to direct heat transfer problems, are defined as the wall estimation of starting and boundary conditions, material characteristics, source and sink terms, and governing equations which are utilizing the temperature distribution at one or more interior sites [2].

In terms of solution stability, inverse issues are much more difficult to solve than direct problems. In mathematics, they are referred to as ill-posed problems. In recent decades, when better computers became available, inverse solution approaches expanded their relevance beyond heat transport problems. For instance, some of the primary applications of inverse heat transfer include the cooling control of electrical equipment, estimation of cooling jet velocity during machining and quenching hardening processes, determination of boundary conditions between mold and molten metal during casting and rolling processes [3], and determination of heat flux on a wall surface exposed to fire or inside the surface of a combustion chamber [4], as well as surfaces where ablation or melting occurs [5]. Other applications of inverse heat transfer include the prediction of the internal wall of reactors, determining the thermal conductivity and external surface conditions during a space vehicle's re-entry, modeling temperature or heat flux distributions at the tool-work interface during machine cutting [6], and solving cooling control problems [7]. Numerous methods for solving inverse heat transfer problems are used, including exact solutions, the inverse transform of the Duhamel integral, the Laplace transformation, the control volume method, Helmholtz equations, finite difference, finite element approximation, digital filter synthesis, Tikhonov regularization, the Elifanov iteration method, conjugate gradient, and Levenberg–Marquardt methods [8]. The Levenberg–Marquardt technique is an iterative inverse algorithm that is used in this research. It is based on minimizing the least-square summation of the error values Jiang and the others. [9] obtained the time-dependent boundary heat flux on a solid bar using the conjugate gradient method with an adjoint equation and zeroth-order Tikhonov regularization approach to make the inverse solution stable. In their work, the finite difference method was used to solve the problem. *Chen et al*. [10] used the inverse approach, they determined the temperature and heat flow distributions at the quenching surface. They enhanced temperature and heat flow estimates using the conjugate gradient approach for a two-dimensional issue in cylindrical dimensions. The governing equations were solved by using finite element methods. *Plotkowski* and *Krane* [11] investigated how to quantify transient heat flow in electro-slag remelting in using inverse heat conduction models. They investigated three ways of inverse heat transfer for industrial use. *Hsu et al*. [12] investigated film-wise condensation on a vertical surface using the inverse problem on wall heat flux estimate. Their inverse technique does not need previous knowledge of an unknown variable's functional form. *Khaniki* and *Karimian* [13] calculated the heat flow absorbed by a satellite surface using temperature data. They devised a basic heat flux sensor in order to investigate the associated potential limits. Additionally, they suggested an inverse solution to the energy equation using temperature data, which produces the heat flux absorbed on the satellite's surface. *Beck et al*. [14] conducted some research into the estimation of heat flux entering the surface of a body using the inverse approach. Their calculation method used the measured temperature data of the internal points.

Liu [15] developed a hybrid mechanism to simultaneously identify the thermal conductivity and heat capacity in an inverse heat flux problem. This mechanism was a combination of genetic algorithms and Levenberg–Marquardt algorithms. *Mohammadiun et al*. [16] used temperature at a site to calculate the time-dependent heat flow. Their approach comprised solving the governing equations through the finite difference technique. *Tai et al.* [17] applied an inverse conduction heat transfer method to estimate the spatial and temporal variation of heat flux on the drilled-hole wall surfaces. Their approach used the internal temperature of the body measured by thermocouples, and the governing equations were solved by the finite element method. *Rahimi et al*. [18] estimated the time-dependent strength of a heat source using temperature distribution at a point in a three-layer system. *Mohammadiun et al*. [19] employed the sequential function definition approach to forecasting heat flow across disintegrating materials' sublimation boundaries. They employed the inverse

approach to forecasting surface thermal boundary conditions. In another study, *Mohammadiun et al*. [20] applied the sequential function specification method to the ablative surfaces. The inverse method has been used in the mentioned study to estimate heat flux at the moving interface.

Wu et al. [21] proposed an inverse algorithm based on the conjugate gradient method to solve the hyperbolic heat conduction problem and estimate the unknown heat flux on an infinite cylinder. The measured internal temperatures were used for this purpose. A technique for inverse estimation, based on a fitting of the displacements, obtained from a combination of static compression and shear traction loads, for the extraction of the equivalent, and static elastic, Hooke's tensor has been proposed by *Mao et al*. [22]. *Trofimovetal*. [23] formulated a theoretical approach based on the property contribution tensors for inverse homogenization procedure in order to reconstruct elastic and electrical/thermal properties of inhomogeneities (matrix) from the known effective properties, matrix (inhomogeneities) properties, and microstructural information. The problem of unknown radiation terms identification in some inverse problems of heat equations with over-specified data measured on the boundary has been investigated by *Mohseni et al*. [24]. In their study, some linear heat equations along with non-linear boundary conditions have been applied to mathematical modeling. An algorithm based on the iteration method and proving its convergence for an inverse problem in heat propagation has been defined by *Capatina et al*. [25]. They used an internal approximation in the space variables and a backward Euler scheme in the time variable to discrete their discussed equations. A new method based on an adaptive-robust minimax algorithm for the inverse problem concerning Fredholm integral equations of the first kind along with input noisy data effects has been developed by *Yanovsky et al*. [26], then they applied this method to the inverse problem in the linear theory of viscoelasticity.

The solution of Navier-Stokes equations is often somewhat difficult mathematically. This is because these equations are non-linear, rendering the superposition theory relevant to potential flow is inapplicable. However, in certain circumstances, an accurate solution to Navier-Stokes may be found by naturally eliminating the non-linear advection factors. Hiemenz was the first to discover the precise answer to the stagnation flow issue [27]. He investigated two-dimensional stagnation flow against a flat plate, assuming that the stagnation flow on the flat plate is laminar, incompressible, and constant. By substituting an appropriate, variable, and converting velocity components to a similarity function, Hiemenz arrived at an ordinary differential equation from which he deduced the velocity and pressure fields near the flat plate.

Wang published the first precise solution to axisymmetric stagnation flow on an infinite cylinder [28]. He presupposed a stationary cylinder with no rotational or axial movement, as well as no suction or blowing on the cylinder wall. A radial axisymmetric flow perpendicular to the axis was assumed. Additionally, due to the symmetry of the free stream with respect to the cylinder axis, all derivatives with respect toϕ (angular direction) and t (time) are zero, simplifying the Navier-Stokes equations in cylindrical coordinates. Gorla investigated the axisymmetric stagnation flow around a cylinder with laminar flow in steady and transient states in a series of studies [29-32]. The effects of uniform axial movement as well as the armonic axial movement of the cylinder were studied in these works. *Cunning et al*. [33] investigated the impact of constant angular velocity cylinder rotation on stagnation flow across the cylinder. The impact of uniform suction and blowing on the cylinder wall was also studied in this study. Due to the rotation of the cylinder, the flow is completely three-dimensional, with velocity extending in ϕ directions. *Takhar et al* [34] The influence of axisymmetric radial stagnation flow on the cylinder was investigated, as well as the effect of variable-speed axial cylinder movement. To arrive at a self-similar solution in their study, the time-dependent functions associated with the free stream and axial velocity of the cylinder are considered to be inverse linear functions of time.

Saleh and *Rahimi* [35-37] found accurate solutions for axisymmetric stagnation flows on an infinite cylinder and the associated heat transfer in instances where the cylinder moves axially and rotationally in time-dependent ways. Additionally, *Mohammadiun et al*. developed self-similar solutions for the radial stagnation point flow and heat transfer of a viscous, compressible fluid impinging on a cylinder in the steady state in a series of investigations [38-41].

They further studied the axisymmetric stagnation flow of a nanofluid on a cylinder for a steady flow when the cylinder wall is exposed to both constant heat flux and constant temperature [42,43]. *Zahmatkesh et al*. [44, 45] determined the entropy generation rate in an axisymmetric stagnation flow of Aluminum oxide nanofluid on a stationary cylinder. The described study also investigates the influence of uniform suction and blowing on the rate of entropy formation, as well as the volume fraction of the nanoparticles. *Hong et al*. [46] applied the similarity solution method to solve the three-dimensional Navier–Stokes equations, governing annular axisymmetric stagnation flow on a moving cylinder. After the reduction of these equations to a set of non-linear ordinary differential equations, an asymptotic solution for small Reynolds numbers has been presented by them.

The effects of non-alignment, i.e., the stagnation and rotation axes are parallel but non-coinciding, in three-dimensional stagnation flow towards a rotating disc, have been studied by Wang [47], and a self-similar solution has been presented in this study. *Song et al*. [48], investigated PSD and optical properties of TiO_2/water suspensions both experimentally and theoretically. *Hatami et al*. [49] studied the natural convection heat transfer of the nanofluids in a circular-wavy cavity to reach the maximum Nusselt number and consequently more heat transfer, a cosine function is assumed for the inner wall equation. Instead of traditional methods, they used RSM to find the optimal geometry for the wavy wall in a time-efficient and accurate way. By applying the FEM and RSM for solving and optimizing the results. *Hatami* and *Safari* [50] studied the natural convection heat transfer of the nanofluids in a wavy-wall cavity when a heated cylinder is located in it to reach the maximum Nusselt number and consequently, more heat transfer and cylinder location are assumed to be variable. *Mosayebidorcheh* and *Hatami* [51] have applied LSM analytical solution to find the solution of 2D modeling of asymmetric peristaltic flow and heat transfer of nanofluids in a wavy wall channel. Comparing the obtained results with numerical solutions confirms the accuracy and validity of the applied analytical method in obtaining both stream function and temperature values. *M. Hatami et al.* [52] presented Some analytical solutions previously for the motion of a particle in plane Couette fluid flow, but they face some shortcomings. they approached a new analytical called Multi-step Differential Transformation Method (Ms-DTM) which has been successfully applied to find the most accurate analytical solution for that problem. *Ghasemi et al*. [53] applied the least squares method and the Galerkin method to solve the problem of peristaltic flow in drug delivery systems. The results were presented to study temperature, nanoparticle fraction, and velocity for various physical parameters such as Brownian motion parameter, thermophoretic parameter, thermal Grashof number, and species Grashof number. *M. Hatami* [54] successfully applied FlexPDE FEM numerical code to find the solution of 2D modeling of natural convection heat transfer of nanofluids in a rectangular cavity containing two heated fins. Two different kinds of nanoparticles are considered, TiO_2 and Al_2O_3 to add to water as base fluid. The effect on nanoparticle type, nanoparticle volume fraction, and height of the fins on the local and average Nusselt number is investigated and it is found that TiO_2 (especially in lower and moderate φ) in the presence of lengthy fins can improve the heat transfer. *M. Hatami* [55] studied the natural convection heat transfer of the nanofluids in a wavy-wall cavity when a heated cylinder is located in it. The cylinder location is fixed in the center of the enclosure while the height and shape of wavy walls are considered to be variable. By applying the FEM for solving the governing equations and using the RSM, the optimized profile is introduced for the wavy wall.

Ali et al. [56] have numerically investigated the interaction of the thermally and hydrodynamically developed flow in a vertical square duct with the magnetic field produced by a nearby-placed wire, under the thermal boundary condition of uniform heat flux across the unit axial length. At a low Rayleigh number, they have observed that the velocity distribution across any cross-section of the duct (parallel to the horizontal or vertical axis), is almost parabolic.

Hatami and *Ganji* [57] successfully applied the analytical approaches, Differential Transformation Method with Padé approximation (DTM-Padé) and quadrature method (DQM), to produce an accurate analytical solution for the motion of a particle in a forced vortex. The radial position, angular velocity, and radial velocity of the particle were calculated and depicted. *Pourmehran et al*. [58] aimed to investigate the problem of heat and fluid flow analysis for nanofluid in MCHS by least square and numerical methods based on saturated porous medium then find the best nanoparticle and

optimize the nanoparticle size, nanoparticle volume fraction, volume flow rate, and inertial force parameter by impression on the Nusselt number and total thermal resistance *via* Central Composite Design (CCD). Influences of nanoparticle volume fraction, volume flow rate, inertial force parameter, nanoparticle size, and channel width on temperature distribution, velocity, Nusselt number, total thermal resistance, and friction factor were considered. *Ahmad et al*. [59] presented a comprehensive analysis of motile microorganisms and activation energy in the flow of pure as well as hybrid nano liquids subject to Darcy Forchheimer medium. The use of a porous medium not only stables the flow but also maintains the thermal characteristics of the fluid. The bioconvection phenomenon is also eminent in the augmentation of the heat transfer characteristics. MATLAB software is used to simulate the problem. *Ahmad et al.* [60] studied the bioconvective flow of gyrotactic microorganisms and nanofluids through a porous media. The flow is taken over a nonlinear expanding/shrinking surface. Bioconvection flows of microbes together with nanoparticles have many useful employments in several fields of science and biotechnology. The system of flow model equations is initially simplified by the similarity transformations, and then, a successive over-relaxation scheme is used to solve the resultant system numerically. *Ahmad et al*. [61] believe and object that the specific rate of heat transfer plays an important role in many engineering systems as it can affect the quality of the product. A specific heat-transfer rate is essentially required in many energy systems, for example, metal expulsion, nuclear system cooling, refrigeration, thermal storage, cooling generators, and so on. The amalgamation of manganese zinc ferrites ($MnZnFe_2O_4$) and silver (Ag) in kerosene oil can assist in increasing the heat transfer rate. *Ali et al*. [62] have formulated a mathematical model for incorporating the impact of wall slip in the rotating EMHD flow of a power-law fluid in a microchannel. They have numerically solved the governing PDEs in dimensionless form employing the fully implicit numerical scheme. Having confirmed the accuracy of the computational procedure, a comprehensive study has been carried out. *Ali et al*. [63] studied how the Nusselt number, temperature profiles, and velocity distributions for the fully developed nanofluid flow in a vertical rectangular duct are affected by the magnetic field produced by a nearby placed dipole. Governing equations are discretized using a finite volume approach, and the algebraic system thus obtained is iteratively solved. The computational technique is rigorously validated by comparing our numerical results with the existing scientific literature for a limiting case of pressure-gradient-driven flow in the square duct in the absence of any dipole. An experimental investigation of heat transfer of Fe_2O_3/Water nanofluid in a double pipe heat exchanger has been performed by *Aghayariet al.* [64]. *Aghayari et al.* applied the artificial neural network (ANN) to predict the thermal conductivity of nanofluid at different temperatures and volume fractions.[65]. *Habibi et al*. [66] investigated the viscosity uncertainty in the floating-axis fluid flow and heat transfer along a horizontal hot circle cylinder immersed in a cold Al_2O_3 water nanofluid. *Nematollahzadeh et al*. have presented an exact analytical solution for the convective heat transfer equation from a semi-spherical fin. They compared exact solutions with numerical results such as the finite difference method and midpoint method with Richardson extrapolation [67]. *Montazeri et al* [71] calculated time-dependent heat flux in the stagnation points of impinging flow on the circular cylinder by an inverse method.

As can be seen, inverse Heat transfer in the area of the impinging flow's stagnation zone has not been examined before. For the first time, this study proposes a numerical code based on the Levenberg–Marquardt technique for solving the inverse time-dependent boundary temperature of an axisymmetric stagnation flow on a cylinder with uniform suction blowing. The approach makes use of a point's temperature distribution and a semi-similar solution. At each time step, the governing equations are transformed into a system of coupled ordinary differential equations, which are solved by using the tri-diagonal matrix algorithm after being discretized, using the implicit finite difference technique (TDMA). The sensitivity of the model to noisy data is examined. The findings reveal that the suggested strategy is very stable in the presence of noisy data.

All articles in the field of Stagnation point flow on the cylinder or flat plate are the only direct problems with known boundary conditions (known wall temperatures) but in this research, for the first-time unknown boundary condition (unknown time-dependent wall Temperature) has been estimated by using only one

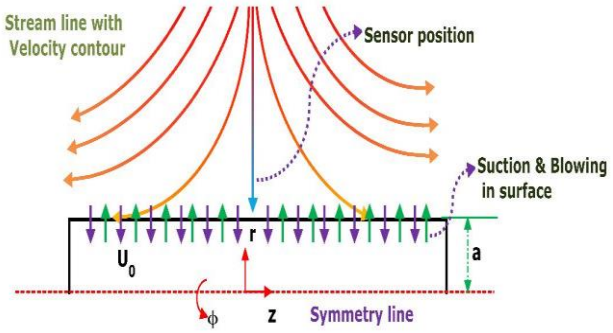

Fig. 1: The geometry of the problem and the location of the sensor

sensor located in the fluid field there this problem has been solved by the inverse method (Levenberg–Marquardt Method). In the similarity solution field, all the papers are direct solutions and there is not any paper witch used the inverse method coupled with the similarity solution technique there the novelty of this paper is the inverse solution of this kind of problem. Since in many industrial applications, it is not possible to insert the sensor on the wall to measure the temperature of the wall, the sensor can be inserted in another place and the wall temperature distribution can be obtained by inverse analysis (Determining of unknown boundary condition).

THEORETICAL SECTION

Problem formulation

A. Direct solution

Fig. 1 illustrates the geometry of this issue. The flow is axisymmetric in cylindrical coordinates(r, z), with matching velocity components (u, w), as shown. On the cylinder's exterior surface, a time-dependent temperature and uniform transpiration are applied. Using the temperature distribution at a location, we seek to calculate the unknown wall temperature $T_w(t)$ within $0 \le t \le t_f$ inside. There is a chance that the data provided includes noise. The numerical code calculates the temperature distribution using the semi-similar solution approach. By converting partial differential equations to ordinary differential equations and solving them numerically, using dimensionless radius and transferring functions, this approach converts partial differential equations to ordinary differential equations.

Several annular jet flows uses include the following: an examination of centrifugal machinery movement, heating and cooling operations, activating and deactivating industrial machines, pressure-lubricated bearings, and cooling of drilling tools and punching instruments.

B. Governing equations

As shown in Fig. 1, the flow is considered in cylindrical coordinate (r,z) with corresponding velocity components (u, w). The flow is assumed incompressible and in a transient state. Dimensionless surface diffusion is $S = U_o/\bar{k}a$ In cylindrical dimensions, assuming axial symmetry; the governing equations will be as follows [35,36]:

Conservation of mass

$$\frac{\partial}{\partial r}(ru) + r\frac{\partial w}{\partial z} = 0 \tag{1}$$

In the direction of r, the momentum equation is as follows:

$$\frac{\partial u}{\partial t} + u\frac{\partial u}{\partial r} + w\frac{\partial u}{\partial z} = -\frac{1}{\rho}\frac{\partial p}{\partial r} + \upsilon\left(\frac{\partial^2 u}{\partial r^2} + \frac{1}{r}\frac{\partial u}{\partial r} - \frac{u}{r^2} + \frac{\partial^2 u}{\partial z^2}\right) \tag{2}$$

Momentum equation in z-direction

$$\frac{\partial w}{\partial t} + u\frac{\partial w}{\partial r} + w\frac{\partial w}{\partial z} = -\frac{1}{\rho}\frac{\partial p}{\partial z} + \upsilon\left(\frac{\partial^2 w}{\partial r^2} + \frac{1}{r}\frac{\partial w}{\partial r} + \frac{\partial^2 w}{\partial z^2}\right) \tag{3}$$

In the above equations,$\rho$and $\upsilon = \frac{\mu}{\rho}$ denotes the fluid density and its kinematic viscosity.

Conservation of energy

$$\frac{\partial T}{\partial t} + u\frac{\partial T}{\partial r} + w\frac{\partial T}{\partial z} = \bar{\alpha}\left(\frac{\partial^2 T}{\partial r^2} + \frac{1}{r}\frac{\partial T}{\partial r} + \frac{\partial^2 T}{\partial z^2}\right) \tag{4}$$

Where $\bar{\alpha} = \frac{k}{\rho C_P}$is the thermal diffusivity coefficient of the fluid.

The following are the boundary conditions for momentum equations:

$$r = a \; : \; u = -U_0 \, , w = 0 \tag{5}$$

$$r \to \infty \; : \; \frac{\partial u}{\partial r} = -\bar{k} \, , w = 2\bar{k}z \tag{6}$$

Eq. (5) are the requirements for transpiration and no-slip boundary conditions of a viscous fluid at the wall. Eq. (6) are derived from the inviscid potential flow solution. The first term in Eq. (6) implies that the gradient of velocity u in distant regions is similar to that in potential

flow. The second element in Eq. (6) represents the fact that the viscous fluid velocity w is equal to the velocity of potential flow at suitably distant positions from the cylinder wall.

The followings are the boundary conditions and initial conditions for solving the energy equation.

$$\begin{aligned} &r = a: T = T_w(t) \\ &r \to \infty: T = T_\infty \\ &t = 0: T(r,0) = T(r)_{steady-state} \end{aligned} \quad (7)$$

Where $T_w(t)$ is the time-dependent wall temperature. Also, T_∞ is the constant temperature of the free stream.

The variables in the governing equations can be reduced. Using the inviscid solution patterns of Eq. (6) and multiplying them by appropriate transfer functions, the below equations are proposed to reduce Navier-Stokes equations to dimensionless semi-similar equations:

$$u=-\bar{k}\frac{a}{\sqrt{\eta}}f(\eta,\tau), w=2\bar{k}f'(\eta,\tau)z, p=\rho\bar{k}^2a^2P \quad (8)$$

Where $\tau = 2\bar{k}t$ and $\eta = (\frac{r}{a})^2$ are dimensionless time and radius, respectively, and ( )' introduces derivative with respect to the variable η. Eq. (8) satisfy the continuity equation automatically, and by substituting them into momentum equations in the z and r directions at each time step, the ordinary differential equation or calculating f is derived, as shown below:

$$\eta f''' + f'' + Re[1 - (f')^2 + ff'' - \frac{\partial f'}{\partial \tau}] = 0 \quad (9)$$

Where $Re = \frac{\bar{k}a^2}{2\upsilon}$ is the Reynolds number Using Eqs. (5) and (6), the boundary conditions for Eq. (9) are obtained as:

$$\begin{aligned} &\eta=1: f=S=\frac{U_0}{\bar{k}a}, f'=0 \\ &\eta \to \infty: f' = 1 \end{aligned} \quad (10)$$

The dimensionless temperature $\theta(\eta,\tau)$ is used to convert the energy equation as follows:

$$\theta(\eta,\tau) = \frac{T(\eta,\tau) - T_\infty}{T_w(\tau) - T_\infty} \quad (11)$$

The energy equation is therefore expressed as follows using Eqs. (8) and (11):

$$\eta\theta'' + \theta' + RePr\left(f\theta' - \frac{\partial\theta}{\partial\tau} - \frac{dT_w(\tau)/d\tau}{T_w(\tau) - T_\infty}\theta\right) = 0 \quad (12)$$

Boundary conditions and initial condition of Eq. (12) are:

$$\begin{aligned} &\theta(1,\tau)=1, \theta(\infty,\tau)=0 \\ &\theta(\eta,0)=\theta(\eta)_{steady\text{-}state} \end{aligned} \quad (13)$$

As can be seen in Fig. 1, the cylinder is impinged by axisymmetric flow in all directions. With the sensor positioned as illustrated in the picture, the Prandtl number is Pr=0.7and the free stream temperature is $T_\infty = 30°C$.

Inverse problem

All inverse solutions involving the minimization of an objective function use an optimization technique. The Levenberg–Marquardt algorithm is one such approach. It is an iterative method for tackling non-linear least squares parameter estimation problems.

This approach is useful for tackling situations involving non-linear parameter estimation. Additionally, it is utilized to solve linear problems that are ill-posed [68]. As a result, it is used in this study to estimate time-dependent wall temperature unknown parameters.

The sensitivity analysis, iteration process, convergence criteria, and calculation algorithms are the primary stages of the Levenberg–Marquardt inverse technique, as detailed below.

The inverse issue is the estimate of temporal fluctuations in wall temperature using sensor-measured transient temperature readings. Thus, $T_w(\tau)$ is an uncertain and time-dependent value, while $Y(\tau)$ is the transient temperature observed at the sensor site during the time period$0 \le \tau \le \tau_f$.

$T_w(\tau) - T_\infty$is estimated using the temperatures observed at the sensor position at times $\tau_i, i = 1,2,...,I$. To solve this inverse issue, we assume that the unknown wall temperature function $T_w(\tau) - T_\infty$ has the following generic linear form:

$$T_w(\tau) - T_\infty = \sum_{j=1}^{N} P_j C_j(\tau) \quad (14)$$

P_j denotes unknown parameters, while $C_j(\tau)$ denotes known trial functions, such as polynomials, splines, and so on, with N parameters. P should be calculated for this inverse heat transfer issue. The disparities between the observed and estimated temperatures are used to define the objective function to be minimized in this case.

There are many techniques for developing an objective function, one of which is the least-squares approach, which is explained below [69]:

$$S_p = \sum_{i=1}^{I} [Y_i - T_i(P)]^2 \quad (15)$$

Where S_p denotes the sum of squares error and thus the objective function, it is necessary to minimize the objective function S_p in order to solve this inverse heat transfer issue and estimate the N unknown parameters P_j,j=1,2,...,N. $P^T=[P_1,P_2,...P_N]$ is the unknown parameter vector in (14). Additionally, $T_i(P) = T(P,\tau_i)$ and $Y_i = Y(\tau_i)$ represent the estimated and observed temperatures at timeτ_i. The approximate temperature $T_i(P)$ is determined by solving the direct problem (9, 12) at the measurement (sensor) location using the unknown factors P_j,j=1,2,...,N.

A. Analysis of sensitivity and computational of the Jacobian matrix

It is beneficial to study the inverse issue and the estimated parameter's sensitivity to unknown parameters before solving it. This study can provide a measure of the optimal temperature sensor location and criteria for the inverse solution's stability. The sensitivity coefficients are defined as follows: (16).

$$J_{ij}=\frac{T_i(P_1,P_2,...,P_j+\varepsilon P_j,...,P_N)-T_i(P_1,P_2,...,P_j,...,P_N)}{\varepsilon P_j} \quad (16)$$

Where $\varepsilon = 10^{-6}$.

The coefficients of (16) are the sensitivity matrix *J*'s members.

$$J(P) = [\frac{\partial T^T(P)}{\partial P}]^T = \begin{bmatrix} \frac{\partial T_1}{\partial P_1} & \frac{\partial T_1}{\partial P_2} & \cdots & \frac{\partial T_1}{\partial P_N} \\ \frac{\partial T_2}{\partial P_1} & \frac{\partial T_2}{\partial P_2} & \cdots & \frac{\partial T_2}{\partial P_N} \\ \vdots & \vdots & \cdots & \vdots \\ \frac{\partial T_I}{\partial P_1} & \frac{\partial T_I}{\partial P_2} & \cdots & \frac{\partial T_I}{\partial P_N} \end{bmatrix} \quad (17)$$

N and *I* denote the total number of unidentified parameters and measurements, respectively.

With tiny sensitivity coefficients, the inverse issue is referred to as an ill-posed problem, which means that it is susceptible to measurement mistakes and hence cannot be accurately estimated. Thus, coefficients with large absolute values are preferable, since they result in stable inverse analysis.

B. The iterative procedure

To minimize the least squares norm given by equations (15), we need to equate to zero the derivatives of *S*(*P*) with respect to each of the unknown parameters $[P_1,P_2,...P_I]$, Such necessary condition for the minimization of *S*(*P*) can be represented in matrix notation by equating the gradient of *S*(*P*) with respect to the vector of parameters *P* to zero, that is:

$$\nabla S(p) = 2[-\frac{\partial T^T(P)}{\partial P}][Y - T(P)] = 0 \quad (18)$$

Where:

$$\frac{\partial T^T(P)}{\partial P} = \begin{bmatrix} \frac{\partial}{\partial P_1} \\ \frac{\partial}{\partial P_2} \\ \vdots \\ \frac{\partial}{\partial P_N} \end{bmatrix} [T_1, \quad T_2, \quad \cdots \quad T_I] \quad (19)$$

The transpose of Equation (19) is the sensitivity matrix which defined by Equation (17) previously. The elements of the sensitivity matrix are called the Sensitivity Coefficients. The sensitivity coefficient *J* is thus defined as the first derivative of the estimated temperature at the time *t*, with respect to the unknown parameter P_j, that is,

$$J_{ij} = \frac{\partial T_i}{\partial P_j} \quad (20)$$

The sensitivity coefficient determined by relation (16) that introduced previously. By using the definition of the sensitivity matrix given by Eq. (17), Eq. (18) becomes:

$$-2J^T(P)[Y - T(P)] = 0 \quad (21)$$

The solution of Eq. (21) for nonlinear estimation problems then requires an iterative procedure, which is obtained by linearizing the vector of estimated temperatures, *T* (*P*), with a Taylor series expansion around the current solution at iteration k. Such a linearization is given by:

$$T(P) = T(P^k) + J^k(P - P^k) \quad (22)$$

Where $T(P^k)$ and J^k are the estimated temperatures and the sensitivity matrix evaluated at iteration *k*, respectively. Eq. (22) is substituted into Eq. (21) and the resulting expression is rearranged to yield the following iterative

procedure to obtain the vector of unknown parameters P [70]:

$$P^{k+1} = P^k + [(J^k)^T J^k]^{-1}(J^k)^T[Y - T(P^k)] \quad (23)$$

Such method is actually an approximation for the Newton (or Newton-Raphson) method. We note that Eq. (10), require the matrix J^TJ to be nonsingular, or

$$|J^TJ| \neq 0 \quad (24)$$

Where $|\cdots|$ is the determinant. If the determinant of J^TJ is zero, or even very small, the parameters Pj, for j = 1, ..., N, cannot be determined by using the iterative procedure of equation (24). Problems satisfying $|J^TJ|$=0 are denoted ill-conditioned. Inverse heat transfer problems are generally very ill-conditioned, especially near the initial guess used for the unknown parameters, creating difficulties in the application of the equation [24]. The Levenberg-Marquardt Method [68] alleviates such difficulties by utilizing an iterative procedure in the form:

$$P^{k+1}=P^k+\left[(J^k)^TJ^k+\mu^k\Omega^k\right]^{-1}(J^k)^T\left[Y-T(P^k)\right] \quad (25)$$

Where μ^k is the damping parameter, a positive scalar value, and Ω^k is a diagonal matrix. $\mu^k\Omega^k$ is the damping parameter matrix utilized to moderate the oscillations and instabilities that contribute to the inverse problem's ill-conditioned nature. At the start of the iteration process, an enormous value is assumed for this parameter since the issue is often ill-posed around the initial estimate made for the iteration process. This parameter may differ significantly from the real values. As a result, at the beginning of the iteration, the Levenberg–Marquardt method tends toward the steepest descent method in which a tiny step is taken in the negative gradient direction. Then, as the iteration continues, the value μ^k is reduced; making the Levenberg–Marquardt method performs similar to the Newton-Gauss method.

C. Convergence criterion

To achieve convergence of Eq. (18), a convergence criterion is required to signal the end of the Levenberg-Marquardt method's iteration process. This criterion prevents the observed errors from expanding and, in conjunction with the iteration method used for regularization, converts the inverse problem to a well-conditioned issue. This research uses the following convergence criterion:

$$S(P^{k+1}) < \varepsilon_1 \quad (26)$$

Where ε_1 is the user-specified tolerance for terminating the minimization procedure, depending on the degree of distortion in the measured data. This criterion determines if the obtained solution sufficiently minimizes the goal function.

D. Computational algorithm

Assuming a starting assumption of P^0 for the unknown parameter vector P and k=0 and $\mu_0 = 0.05$, the following stages outline the Levenberg–Marquardt algorithm:

1. Solve the direct problem using the initial guess for P^k, i.e. the initial guess for wall temperature, to obtain the temperature vector $T(P^k)=(T_1,...,T_I)$.
2. Calculate $S(P^k)$ using Equation (15).
3. Calculate the sensitivity matrix J^k defined by Eq. (17) and diagonal matrix Ω^k using the current P^k values. To calculate the diagonal matrix Ω^k, use the following relation.

$$\Omega^k = diag[(J^k)^TJ^k] \quad (27)$$

4. Solve the following linear system of algebraic equations, obtained from the iteration of Eq. (25).

$$[(J^k)^TJ^k + \mu^k\Omega^k]\Delta P^k = (J^k)^T[Y - T(P^k)] \quad (28)$$

5. Calculate the new estimation of P^{k+1} as:

$$P^{k+1} = P^k + \Delta P^k \quad (29)$$

6. Solve the direct problem using the new estimate P^{k+1} and get the vector $T(P^{k+1})$ and then calculate $S(P^{k+1})$ using Equation (15).
7. If $S(P^{k+1}) \geq S(P^k)$, then substitute μ^k with $10\mu^k$ and return to step 4.
8. If $S(P^{k+1}) < S(P^k)$, accept the new estimate P^{k+1} and substitute μ^k with $0.1\mu^k$.
9. Check the stopping criterion, Eq. (26). Stop the iterative procedure if it is satisfied. Else, substitute k with k+1 and return to step 3.

RESULTS AND DISCUSSION

The primary objective of this study is to estimate an unknown wall temperature in stagnation point flow on a cylinder using the Levenberg-Marquardt approach in the absence of knowledge about unknown functions.

As shown in the previous section, the Levenberg-Marquardt method has been applied to estimate the

unknown wall temperature at the impinging flow's stagnation area on the circular cylinder. Since no information is available on the unknown boundary condition, a ninth-order polynomial with unknown coefficients has been used for estimating wall temperature. The aim of this study is to determine the unknown coefficients by curve fitting based on the Levenberg-Marquardt algorithm.

The governing equations are discretized using the implicit Finite Difference approach. The time variable is assumed to be dimensionless, whereas the time step is taken to be $\Delta\tau = 0.01$. The boundary temperature is calculated and the noise data sensitivity is tested in this research utilizing the observed temperature at a point. Noisy data are created by the use of (30). The suggested approach's stability under various noise levels is evaluated by using $\sigma = 0.01T_{max}$ and $\sigma = 0.03T_{max}$.

$$Y(\tau_i) = Y_{ex}(\tau_i) + \omega\sigma \tag{30}$$

The above equationσ is the standard deviation of the measurement errors and ω is a random variable with normal distribution, zero mean, and unitary standard deviation. For the present study, $-2.576 \le \omega \le 2.576$. Additionally, the relation $\varepsilon_1 = \sigma^2\tau_f$ is examined for noisy data, where $\tau_f$is the final dimensionless time parameter. To determine the suggested algorithm's correctness, the exponential, sinus–cosine, triangular, and trapezoidal functions are studied for$T_w(\tau) - T_\infty$.

The following sections provide detailed explanations of the time-dependent wall temperature:

$$T_w(\tau) - T_\infty = 30e^{\tau} - 5.55e^{2\tau} \tag{31}$$

$$T_w(\tau) - T_\infty = 50\,sin(\tau) + 20\,cos(3\tau) \tag{32}$$

$$T_w(\tau) - T_\infty = \begin{cases} 20 + 30\tau for 0 < \tau \le 0.6 \\ 49.7 - 20\tau for \tau > 0.6 \end{cases} \tag{33}$$

$$T_w(\tau) - T_\infty = \begin{cases} 30 for 0 < \tau \le 0.2 \\ 10 + 100\tau for 0.2 < \tau \le 0.4 \\ 50 for 0.4 < \tau \le 0.6 \\ 110 - 100\tau for 0.6 < \tau \le 0.8 \\ 30 for \tau > 0.8 \end{cases} \tag{34}$$

Additionally, the temperature history at points η_1 is shown for both the actual and estimated values.

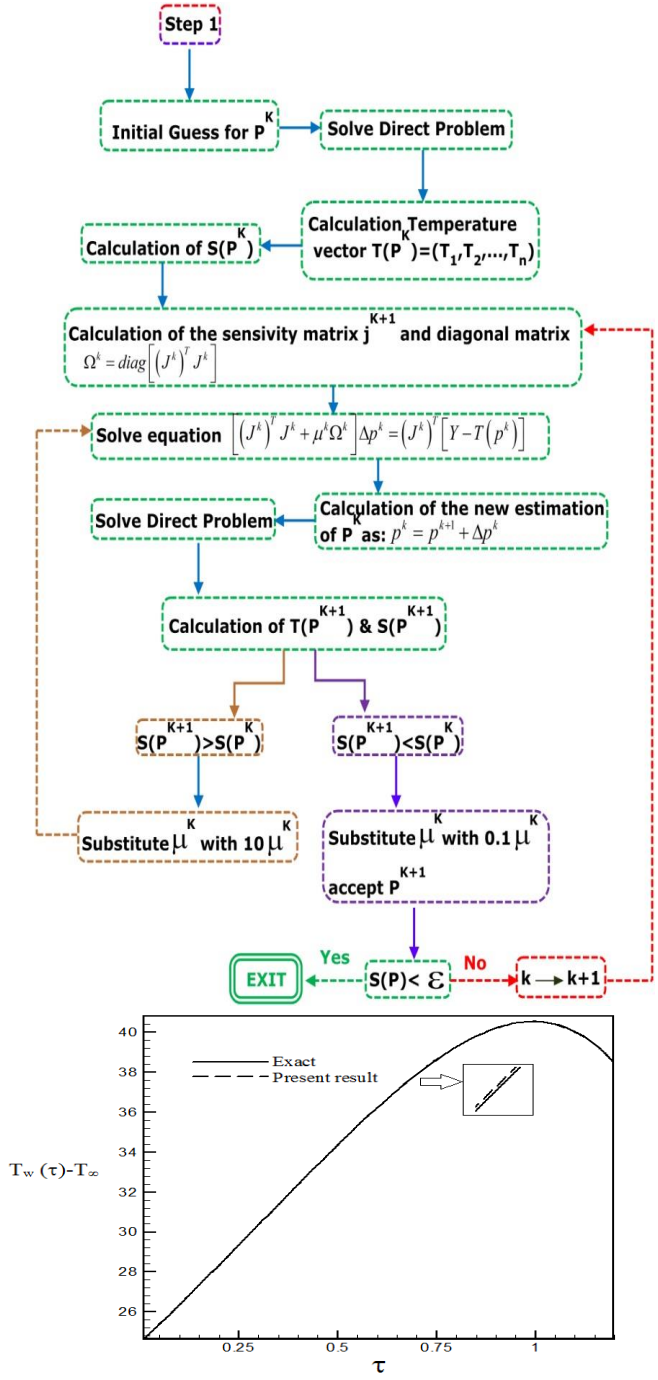

Fig.2: Exact wall temperature vs. calculated wall temperature with Re=100 and S=-0.1 in the form of an exponential curve

Figs. 2-5 are presented to confirm the performance of the inverse algorithm, in this case, the exact wall temperature function is $T_w(\tau) - T_\infty = 30e^{\tau} - 5.55e^{2\tau}$and as can be seen, there is a good overlap between the presented results and the exact function of wall temperature.

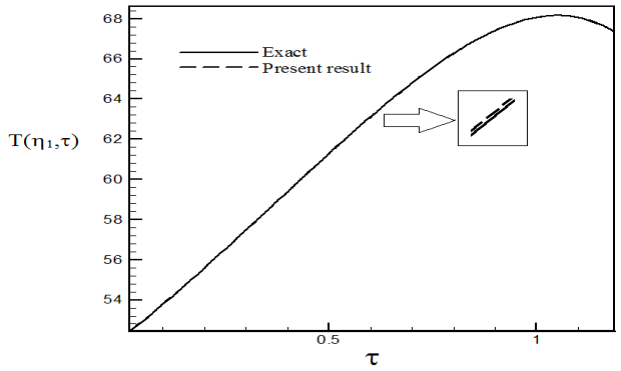

Fig. 3: Temperature history at point η1=1.02 with Re=100 and S=-0.1 in the form of an exponential function for calculated wall temperature vs. exact wall temperature

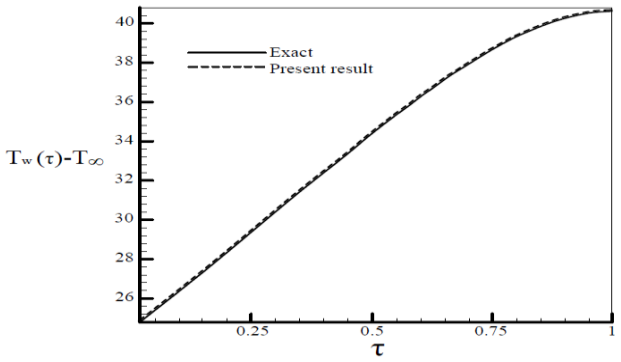

Fig. 6: Exponential function of the calculated wall temperature with Re=100 and S=0.1 vs. the actual wall temperature

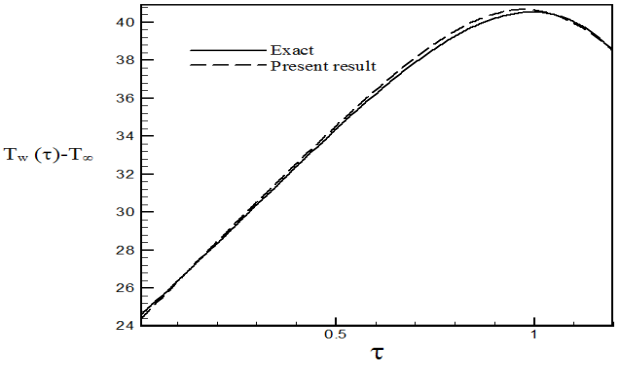

Fig. 4: Exact wall temperature vs. calculated wall temperature with Re=100 and S=-0.1 using noisy data ($\sigma = 0.01T_{max}$ vs. calculated wall temperature using an exponential formula

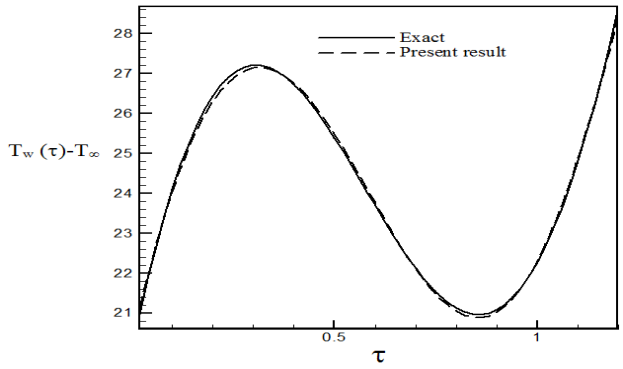

Fig. 7: The estimated wall temperature with Re=300 and S=-0.1 is plotted against the actual wall temperature using a sinus–cosines function

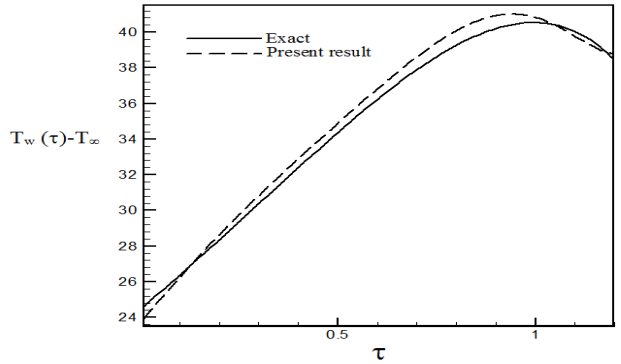

Fig. 5: Calculated wall temperature using noisy data with Re=100 and S=-0.1. ($\sigma = 0.03T_{max}$vs the precise wall temperature as an exponential function

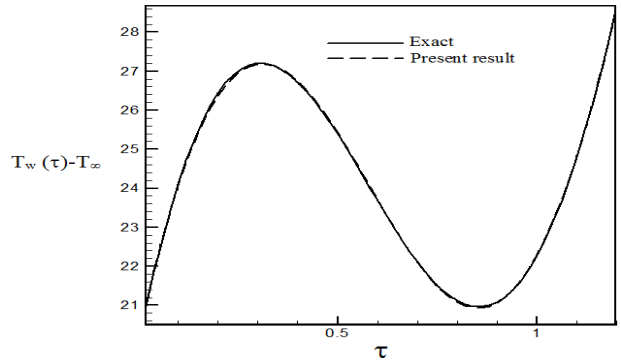

Fig. 8: Conversion of the calculated wall temperature with Re=300 and S=0.5 to the precise wall temperature using a sinus–cosines function

As shown in the previous section, the Levenberg-Marquardt method has been applied to estimate the unknown boundary condition (time- dependent temperature. wall temperature) in the stagnation region of the impinging flow on the circular cylinder. Since no information is available on the unknown boundary condition, ninth-order polynomial ($T_w(\tau) - T_\infty = \sum_{j=0}^{9} P_j \tau^j$) with unknown coefficients has been used for estimating wall heat.

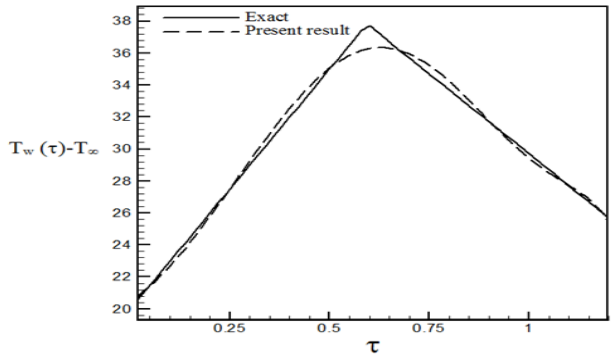

Fig. 9: The calculated wall temperature with Re=150 and S=-0.1 is plotted against the actual wall temperature using a triangular function

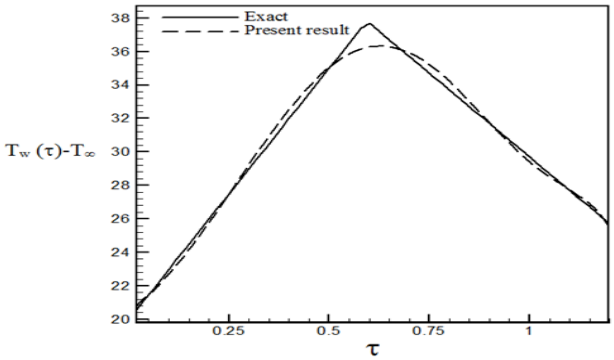

Fig. 10: The calculated wall temperature with Re=150 and S=0.5 vs the actual wall temperature as a triangle curve

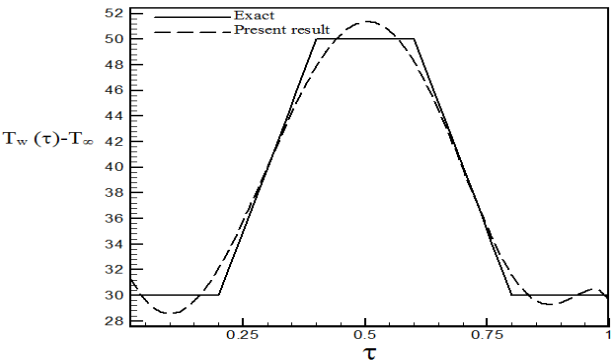

Fig. 11: A trapezoidal curve representing the calculated wall temperature with Re=300 and S=-0.1 vs. the exact wall temperature

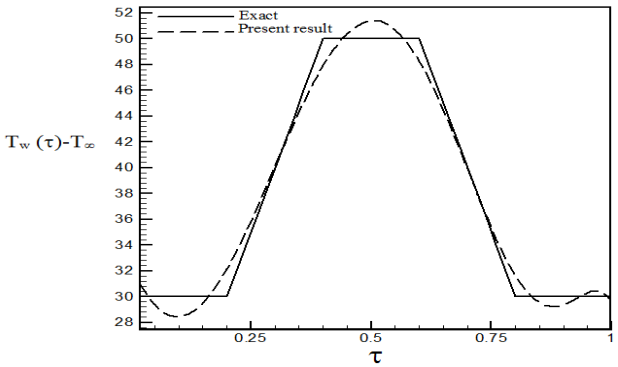

Fig.12: Comparison of calculated wall temperature with Re=300 and S=0.5 to actual wall temperature using a trapezoidal function

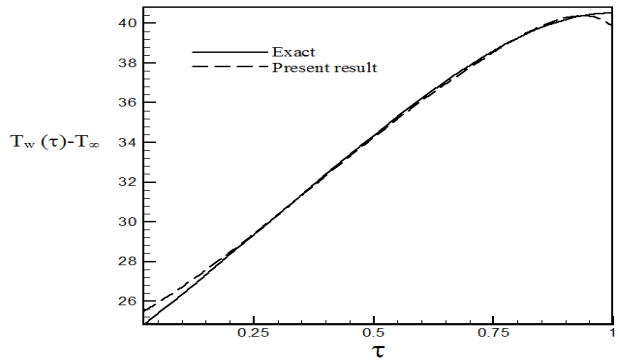

Fig. 13: Exact wall temperature vs. calculated wall temperature with Re=100 and S=0.1 using noisy data $(\sigma = 0.01T_{max})$

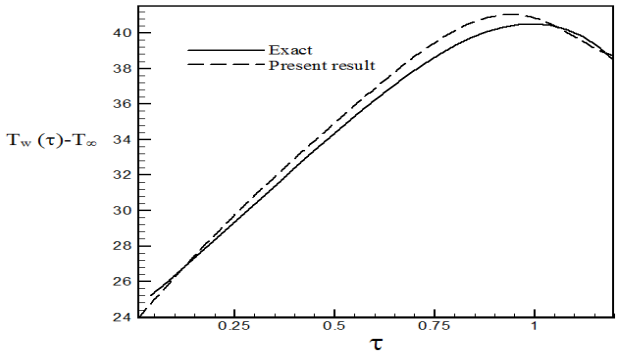

Fig.14: Exact wall temperature vs. calculated wall temperature with Re=100 and S=0.1 using noisy data $(\sigma = 0.03T_{max})$

The aim of this method is to determine the unknown coefficients of the proposed polynomial by curve fitting based on the Levenberg-Marquardt algorithm.

Maximum and minimum values of the $|J_{ij}|$ for the case of Re=100 and S=-0.1 are 0.1693 and 2.8×10^5 respectively. The results show that in the initial times, the sensitivity to the P_0 parameter is lower compared to other parameters because it has a higher sensitivity coefficient and the sensitivity coefficient of other parameters is almost equal to zero this means that in the initial times, the estimated parameters are not suitable for estimating unknown functions but in later times, the sensitivity coefficient of P_0

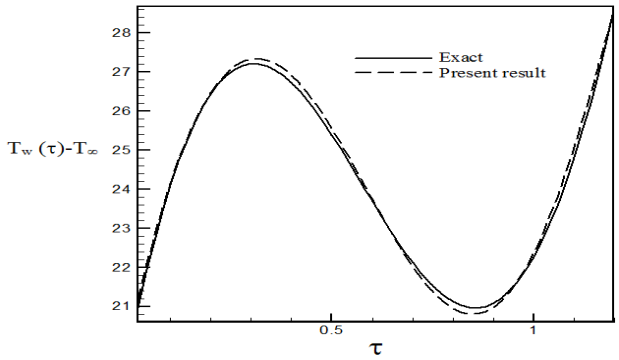

Fig.15: Calculated wall temperature with Re=300 and S=-0.1 using noisy data ($\sigma = 0.01T_{max}$vs. precise wall temperature as a sinus–cosines function

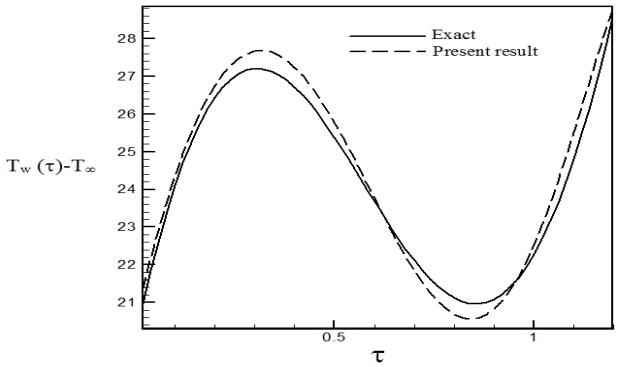

Fig.16: Calculated wall temperature with Re=300 and S=-0.1 using noisy data ($\sigma = 0.03T_{max}$vs. precise wall temperature as a sinus–cosines function

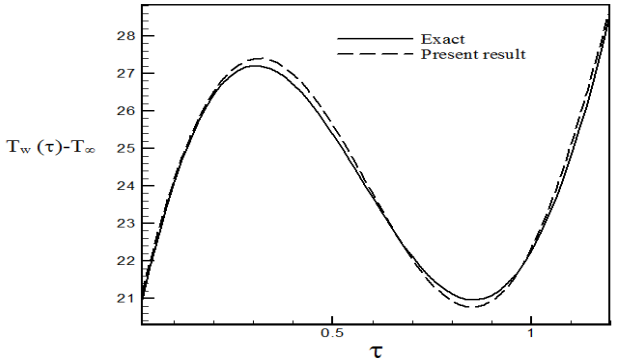

Fig.17: Calculated wall temperature with Re=300 and S=0.5 using noisy data ($\sigma = 0.01T_{max}$ vs. precise wall temperature as a sinus–cosines function

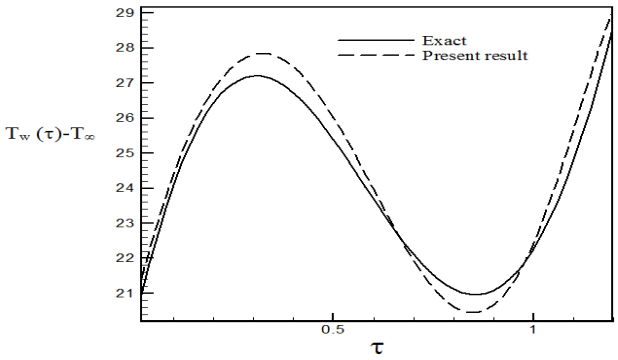

Fig. 18: Calculated wall temperature with Re=300 and S=0.5 using noisy data ($\sigma = 0.03T_{max}$vs. the precise wall temperature as a sinus–cosines function

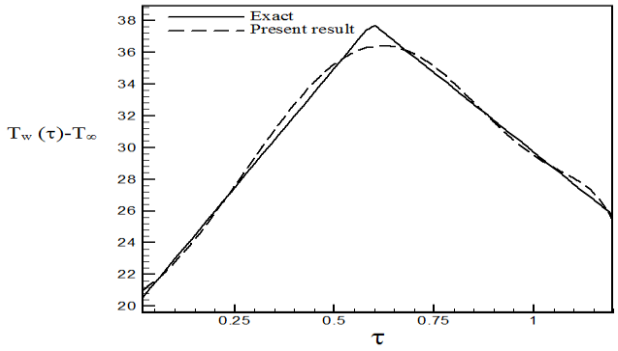

Fig. 19: Calculated wall temperature with Re=150 and S=-0.1 using noisy data ($\sigma = 0.01T_{max}$vs. the precise wall temperature as a triangle function

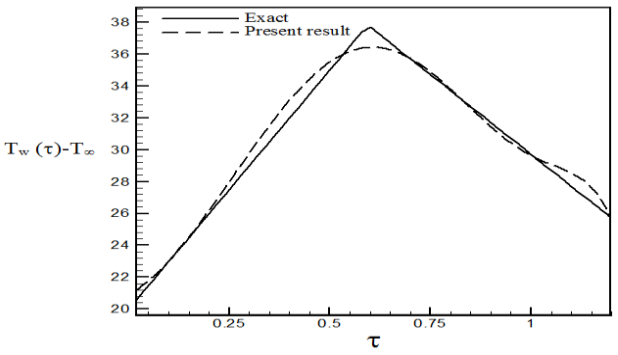

Fig. 20: Calculated wall temperature with Re=150 and S=-0.1 using noisy data ($\sigma = 0.03T_{max}$vs. the precise wall temperature as a triangle function

decreases and in contrast, the sensitivity coefficient of other parameters increases and leads to convergence of iteration method. Figs. 6 to 12 illustrate the aforementioned functions as well as those derived using the inverse approach for chosen Reynolds numbers, followed by the inverse solution for the noisy data. As predicted, in circumstances where triangle and trapezoidal functions are used to estimate the curves, sharp corner points complicate estimation and increase the RMS error. In the case of suction at the wall (S>0), by increasing the temperature

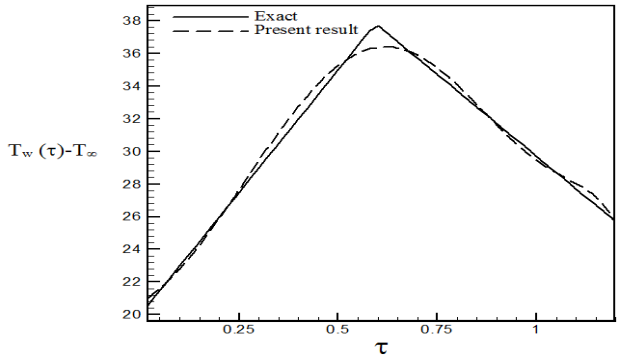

Fig. 21: Calculated wall temperature with Re=150 and S=0.5 using noisy data ($\sigma = 0.01T_{max}$vs. the precise wall temperature as a triangle function

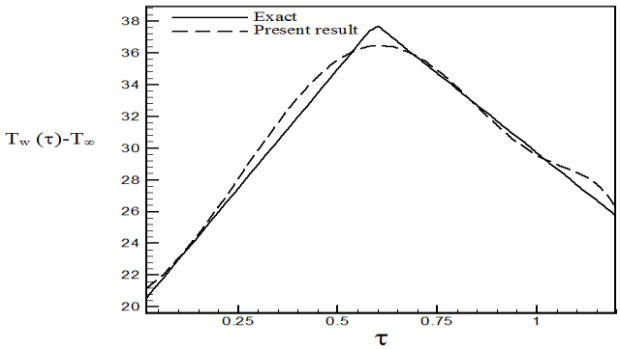

Fig. 22: Calculated wall temperature with Re=150 and S=0.5 using noisy data ($\sigma = 0.03T_{max}$vs. the precise wall temperature as a triangle function

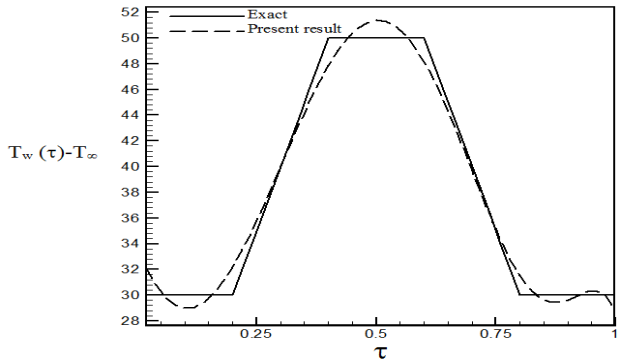

Fig. 23: Calculated wall temperature with Re=300 and S=-0.1 using noisy data ($\sigma = 0.01T_{max}$vs. the precise wall temperature as a trapezoidal function

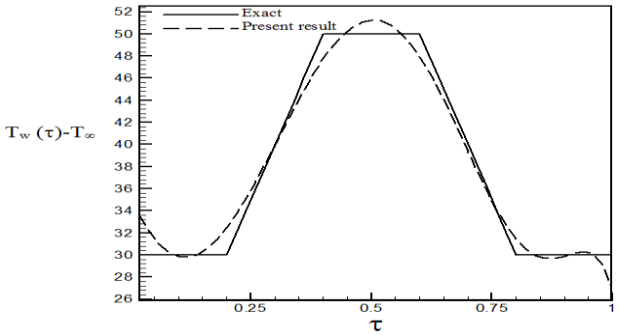

Fig.24: Calculated wall temperature with Re=300 and S=-0.1 using noisy data ($\sigma = 0.03T_{max}$vs. the precise wall temperature as a trapezoidal function

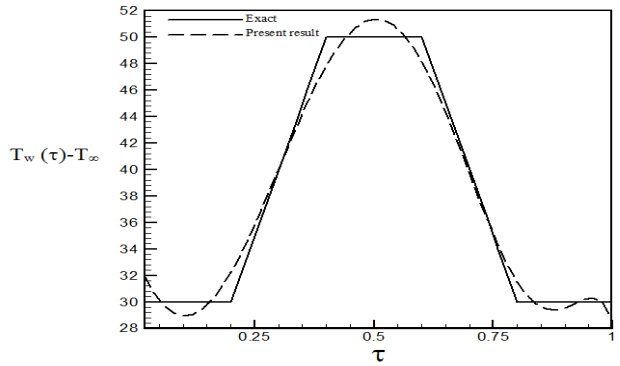

Fig.25: Calculated wall temperature with Re=300 and S=0.5 using noisy data ($\sigma = 0.01T_{max}$vs. the precise wall temperature as a trapezoidal function

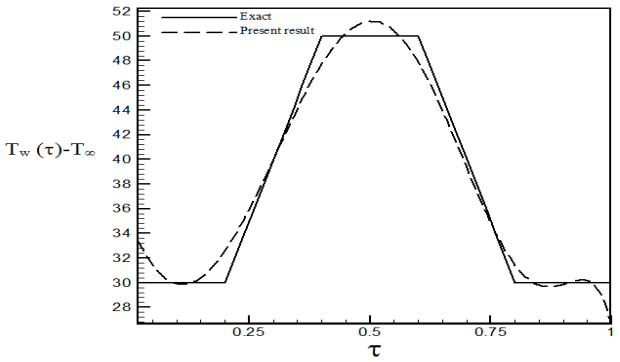

Fig.26: Calculated wall temperature with Re=300 and S=0.5 using noisy data ($\sigma = 0.03T_{max}$vs. the precise wall temperature as a trapezoidal function

gradient at the cylinder surface and decreasing the thermal boundary layer thickness, the heat transfer rate is increased, and estimation of unknown functions becomes more accessible than before. Nevertheless, as expected, surface blowing(S<0) acts completely reverse.

Different function forms and various values of Reynolds numbers have been used to investigate the stability and the accuracy of the solution method. Since our aim has been to examine different ranges of Reynolds numbers and surface transpiration rates we considered the different combinations of Re and S. As can be seen in the Figures. related to temperature history, surface blowing causes

Table1: RMS error for the exponential function of wall temperature

Dimension less transpiration	e_{RMS}		
	σ=0	σ=0.01Tmax	σ=0.03Tmax
S=-0.1	0.0019	0.108	0.209
S=0.1	0.0021	0.127	0.293

Table 2: RMS error for sinus–cosines function of wall temperature

Dimension less transpiration	e_{RMS}		
	σ=0	σ=0.01Tmax	σ=0.03Tmax
S=-0.1	0.0069	0.058	0.237
S=0.5	0.0038	0.061	0.246

Table 3: RMS error for the triangular function of wall temperature

Dimension less transpiration	e_{RMS}		
	σ=0	σ=0.01Tmax	σ=0.03Tmax
S=-0.1	0.233	0.287	0.388
S=0.5	0.221	0.304	0.386

Table 4: RMS error for the trapezoidal function of wall temperature

Dimension less transpiration	e_{RMS}		
	σ=0	σ=0.01Tmax	σ=0.03Tmax
S=-0.1	0.316	0.379	0.427
S=0.5	0.313	0.376	0.425

more heat transfer from the hot wall to the fluid and increased the fluid temperature whereas surface suction absolutely acts vice versa and leads to a decrease in the fluid temperature. The Root Mean Square (RMS) error is a convenient metric for assessing the accuracy of Levenberg–Marquardt parameter estimate.:

$$e_{RMS}=\sqrt{\frac{1}{I}\sum_{i=1}^{I}[T_w(\tau_i)_{est}-T_w(\tau_i)_{ex}]^2} \quad (35)$$

Where $T_w(\tau_i)_{est}$is the estimated function at time τ_i, $T_w(\tau_i)_{ex}$denotes the precise function at time τ_i, and I denote the total number of measurements. The Root Means Square (RMS) error is a measure of the difference between the estimated and actual values of a function. The collected findings indicate that the trapezoidal function has the biggest RMS error owing to the function curve's sharp corner points. As it is shown by the accompanying curves corner points. As it is shown by the accompanying curves and tables, as well as the computed errors, the suggested technique is deemed to have an acceptable degree of accuracy.

The influence of noisy data on the estimate of time-dependent wall temperatures is seen in Figs. 13 to 26. The deviation between the estimated and real wall temperatures increased as the standard deviation of measurement errors increased from σ=0.01Tmax to σ=0.03Tmax, and as can be seen, noisy data results in a greater deviation of the obtained results than exact data, because according to Eq. (30), noise in measured data by the sensor results in error in Eq. (15).

Additionally, the RMS errors associated with these findings are shown in Tables 1 to 4.

As shown in the tables, the error values for estimating triangular and trapezoidal functions are greater than those for exponential and Sinus-cosines functions, owing to the most difficult to recover using inverse analysis. fact that the high gradient changes are not completely recovered by the estimation function, and some oscillations near the singular points are observed. We observe that functions with discontinuities and sharp comers (i.e., discontinuities in their first derivatives) are Generally, the outcomes are dependent on the physical nature of the issue, the number of estimated parameters, the starting assumption, and so forth.

CONCLUSIONS

The study presents a semi-similar solution to the axisymmetric inverse issue for the estimate of time-dependent wall temperature based on the observed temperature distribution at a location in the permeable wall's stagnation zone. The ninth-order polynomials function with coefficients produced via the Levenberg–Marquardt parameter, estimation approach was used to estimate the unknown boundary condition. The RMS error was computed for many samples and it was discovered that the error is the greatest for the trapezoidal function owing to its sharp corners. Additionally, in the majority of situations, the RMS error rises as the rate of surface blowing increases due to the displacement of the thermal boundary layer from the surface. Among the considered functions, the trapezoidal function is the most difficult to fit with the inverse approach and is therefore chosen

to evaluate the algorithm's accuracy. The proposed method in this paper is a general approach that can be applied to inverse heat transfer problems with axisymmetric stagnation flow. Based on the analyzed situations and the fact that no previous knowledge of the structure of the unknown function is needed, as well as the acceptable stability against noisy data, it is concluded that this methodology is an effective way of estimating the time-dependent wall temperature.

Nomenclature

A	Cylinder radius[m]
C	Known trial functions used in Levenberg-Marquardt method
e_{RMS}	Root mean square error
f	Dimensionless function defining velocity field
S	Dimensionless transpiration
S_p	Sum of squares error
I	Number of measurements
J	Sensitivity matrix
$\bar{k}$	Free stream strain rate[1/s]
N	Number of unknown parameters
p	Fluid pressure[N/m^2]
P	Dimensionless pressure
Pr	Prandtel number
P^k	Vector of unknown parameters at current iteration
r,z	Cylindrical coordinates[m]
Re	Reynolds number
T	Temperature [°C]
u	Radial component of the velocity field[m/s]
U_0	Velocity of suction or blowing at the wall[m/s]
w	Axial component of the velocity field[m/s]
t	Time[s]
t_f	Final time[s]
T_∞=	Free stream temperature[°C]
$T_w(t)$	Time-Dependent wall temperature[°C]
T_{max}	Maximum temperature measured by sensor[°C]
Y	Measured transient temperature in the sensor position[°C]
η	Dimensionless radius
θ	Dimensionless temperature
τ	Dimensionless time
μ	Dynamic viscosity [(N.s)/m^2]
μ^k	Damping parameter
υ	Kinematic viscosity[m^2/s]
ρ	Fluid density[kg/m^3]
$\bar{\alpha}$	Fluid thermal diffusivity coefficient[m^2/s]
σ	Standard deviation of measurement errors
ω	Normal distribution
Ω^k	Diagonal matrix
ε_1	Tolerance for stopping the minimization process
$\Delta\tau$	Dimensionless time step
τ_f	Final dimensionless time

Received : Dec.27, 2022 ; Accepted : Mar. 13, 2023

REFRENCES

[1] Huang C.H., Wang P., A Three-Dimensional Inverse Heat Conduction Problem in Estimating Surface Heat Flux by Conjugate Gradient Method, *Int. J. Heat Mass Trans.*, **42(18)**: 3387-3403 (1999).

[2] Shiguemori E.H., Harter F.P., Campos Velho H.F., Dasilva J.D.S., Estimation of Boundary Condition in Conduction Heat Transfer by Neural Networks, *Tendênciasem Matemática Aplicada e Computacional.*, **3**: 189-195 (2002).

[3] Volle F., Maillet D., Gradeck M., Kouachi A., Lebouché M., Practical Application of Inverse Heat Conduction for Wall Condition Estimation on a Rotating Cylinder, *Int. J. Heat Mass Trans.*, **52(2):** 210-221 (2009).

[4] GolbaharHaghighi M.R., Eghtesad M., Malekzadeh P., Necsulescu D.S., Three-Dimensional Inverse Transient Heat Transfer Analysis of Thick Functionally Graded Plates, *Ene. Convers. Manage.*, **50(3)**: 450-457 (2009).

[5] Su J., Neto A., Two Dimensional Inverse Heat Conduction Problem of Source Strength Estimation in Cylindrical Rods, *Applied Mathematical Modeling.*, **25(10)**: 861- 872 (2001).

[6] Hsu P.T., Estimating the Boundary Condition in a 3D Inverse Hyperbolic Heat Conduction Problem, *Applied Mathematics and Computation*, **177(2)**: 453- 464 (2006).

[7] Shi J., Wang J., Inverse Problem of Estimating Space and Time Dependent Hot Surface Heat Flux in Transient Transpiration Cooling Process, *Int. J. Thermal Sc.*, **48(7)**: 1398-1404 (2009).

[8] Ling X., Atluri S.N., Stability Analysis for Inverse Heat Conduction Problems, *Computer Modeling in Engineering & Sciences.*, **13(3)**: 219-228 (2006).

[9] Jiang B.H., Nguyen T.H., Prud'homme M., Control of the Boundary Heat Flux during the Heating Process of a Solid Material, *Int. Commun. Heat Mass Transfer.*, **32(6)**: 728-738 (2005).

[10] Chen S.G., Weng C.I., Lin J., Inverse Estimation of Transient Temperature Distribution in the End Quenching Test, *J. Mater. Process. Technol.*, **86(3)**: 257-263 (1999).

[11] Plotkowski A., Krane M.M., The Use of Inverse Heat Conduction Models for Estimation of Transient Surface Heat Flux in Electroslag Remelting, *J. Heat Transfer.*, **137(3)**: 031301 (2015).

[12] Hsu P.T., Wang S.G., Li T.Y., An Inverse Problem Approach for Estimating the Wall Heat Flux in Film Wise Condensation on a Vertical Surface with Variable Heat Flux and Body Force Convection, *Applied Mathematical Modeling.*, **24(3)**: 235-245 (2000).

[13] Khaniki H.B., Karimian S.M.H., Determining the Heat Flux Absorbed by Satellite Surfaces with Temperature Data, *Journal of Mechanical Science and Technology.*, **28**: 2393-2398 (2014).

[14] Beck J., Blackwell B., Clair C. St., "Inverse Heat Conduction", Wiley, New York, (1985).

[15] Liu F.B., A Hybrid Method for The Inverse Heat Transfer of Estimating Fluid Thermal Conductivity and Heat Capacity, *Int. J. Thermal Sc.*, **50(5)**: 718-724 (2011).

[16] Mohammadiun M., Rahimi A.B., Khazaee I., Estimation of the Time-Dependent Heat Flux Using Temperature Distribution at a Point by Conjugate Gradient Method, *Int. J. Thermal Sci.*, **50(11)**: 2443-2450 (2011).

[17] Tai B.L., Stephenson D.A., Shih A.J., An Inverse Heat Transfer Method for Determining Work Piece Temperature in Minimum Quantity Lubrication Deep Hole Drilling, *J. Manuf. Sci. Eng.*, **134(2)**: 021006 (2012).

[18] Rahimi A.B., Mohammadiun M., Estimation of the Strength of the Time-dependent Heat Source Using Temperature Distribution at a Point in a Three Layer System, *Int. J. Eng.*, **25(4)**: 389-397 (2012).

[19] Mohammadiun H., Molavi H., TaleshBahrami H.R., Mohammadiun M., Real-Time Evaluation of Severe Heat Load Over Moving Interface of Decomposing Composites, *J. Heat Transfer.*, **134(11)**: 111202 (2012).

[20] Mohammadiun M., Molavi H., TaleshBahrami H.R., Mohammadiun H., Application of Sequential Function Specification Method in Heat Flux Monitoring of Receding Solid Surfaces, *Heat Transfer Eng.*, **35 (10)**: 933–941(2014).

[21] WuT. S., LeeH. L., ChangW. J., YangY. C., An Inverse Hyperbolic Heat Conduction Problem in Estimating Pulse Heat Flux with a Dual-Phase-Lag Model, *Int. Commun. Heat Mass Transfer.*, **60**: 1-8 (2015).

[22] Cuadrado D. G., Marconnet A., Paniagua G., Non-Linear Non-Iterative Transient Inverse Conjugate Heat Transfer Method Applied to Microelectronics, *Int. J. Heat Mass Trans.*, **152**: 119503 (2020).

[23] Trofimov A., Abaimov S., Sevostianov I., Inverse Homogenization Problem: Evaluation of Elastic and Electrical (Thermal) Properties of Composite Constituents, *Int. J. Eng. Sci.*,**129**: 34–46(2018).

[24] Mohseni K., Shidfar A., Some Inverse Problems with Explicit Solutions, *Int. J. Eng. Sci.*, **30(3)**: 393–395(1992).

[25] Capatina A., Stavre R., Algorithms and Convergence Results for an Inverse Problem Inheat Propagation, *Int. J. Eng. Sci.* **38 (5)**: 575–587(2000).

[26] YanovskyY. G., BasistovY. A., Linear Inverse Problems in Viscoelastic Continua and Minimax Method for Fredholm Equations of the First Kind, *Int. J. Eng. Sci.*, **34 (11)**: 1221–1245(1996).

[27] Hiemenz K., Die Grenzchicht an Einem in den Gleichformingen Flussigkeitsstrom Eingetauchten Geraden Kreiszylinder, *Dingler'sPolytechn. Journal*, **326**: 391-393 (1911).

[28] Wang C., Axisymmetric Stagnation Flow on a Cylinder, *Q. Appl. Math.*, 32(2): 207-213 (1974).[29] Gorla R.S.R., Nonsimilar Axisymmetric Stagnation Flow on a Moving Cylinder, *Int. J. Eng. Sci.*, **16(6)**: 397-400 (1978).

[30] Gorla R.S.R., Transient Response Behaviour of an Axisymmetric Stagnation Flow on a Circular Cylinder due to Time Dependent Free Stream Velocity, *Int. J. Eng. Sci.*, **16(7)**: 493- 502 (1978).

[31] Gorla R.S.R., Heat Transfer in Axisymmetric Stagnation Flow on a Cylinder, *Appl. Sci. Res.*, **32(5)**: 541-553 (1976).

[32] Gorla R.S.R., Unsteady Viscous Flow in the vicinity of an Axisymmetric Stagnation-Point on a Cylinder, *Int. J. Eng. Sci.*, **17(1)**: 87-93 (1979).

[33] Cunning G.M., Davis A.M.J., Weidman P.D., Radial Stagnation Flow on a Rotating Cylinder with Uniform Transpiration, *J. Eng. Math.*, **33(2)**: 113-128 (1998).

[34] Takhar H.S., Chamkha A.J., Nath G., Unsteady Axisymmetric Stagnation-Point Flow of a Viscous Fluid on a Cylinder, *Int. J. Eng. Sci.*, **37(15)**: 1943-1957 (1999).

[35] Saleh R., Rahimi A. B., Axisymmetric Stagnation-Point Flow and Heat Transfer of a Viscous Fluid on a Moving Cylinder with Time- Dependent Axial Velocity and Uniform Transpiration, *J. Fluids Eng.*, **126(6)**: 997–1005 (2004).

[36] Rahimi A. B., Saleh R., Axisymmetric Stagnation-Point Flow and Heat Transfer of a Viscous Fluid on a Rotating Cylinder with Time- Dependent Angular Velocity and Uniform Transpiration, *J. Fluids Eng.*, **129(1)**: 107–115 (2007).

[37] Rahimi A. B., Saleh R., Similarity Solution of Unaxisymmetric Heat Transfer in Stagnation-Point Flow on a Cylinder with Simultaneous Axial and Rotational Movements, *J. Heat Transfer*, **130(5)**: 054502-1–054502-5 (2008).

[38] Mohammadiun H., Rahimi A.B., Stagnation-Point Flow and Heat Transfer of a Viscous, Compressible Fluid on a Cylinder, *J. Thermophys. Heat Transfer*, **26(3)**: 494-502 (2012).

[39] Mohammadiun H., Rahimi A.B., Kianifar A., Axisymmetric Stagnation-Point Flow and Heat Transfer of a Viscous Compressible Fluid on a Cylinder with Constant Heat Flux, *Sci. Iran., Trans. B*, **20(1)**: 185–194 (2013).

[40] Rahimi A.B., Mohammadiun H., Mohammadiun M., Axisymmetric Stagnation Flow and Heat Transfer of a Compressible Fluid Impinging on a Cylinder Moving Axially, *J. Heat Transfer*, **138(2)**: 022201-1-022201-9 (2016).

[41] Rahimi A.B., Mohammadiun H., Mohammadiun M., Self-Similar Solution of Radial Stagnation Point Flow and Heat Transfer of a Viscous, Compressible Fluid Impinging on a Rotating Cylinder, *Iran. J. Sci. Technol., Trans. Mech. Eng.*, **43(1)**: S141-S153 (2019).

[42] Mohammadiun H., Amerian V., Mohammadiun M., Rahimi A.B.,Similarity Solution of Axisymmetric Stagnation-Point Flow and Heat Transfer of a Nanofluid on a Stationary Cylinder with Constant Wall Temperature, *Iran. J. Sci. Technol. Trans. Mech. Eng.*, **41(1)**: 91-91 (2017).

[43] Mohammadiun H., Amerian V., Mohammadiun M., Khazaee I., Darabi M., Zahedi M.,Axisymmetric Stagnation-Point Flow and Heat Transfer of Nano-Fluid Impinging on a Cylinder with Constant Wall Heat Flux, *Thermal Science.*, **23 (5)**: 3153-3164 (2019).

[44] Zahmatkesh R., Mohammadiun H., Mohammadiun M., Dibaei Bonab M.H., Investigation of Entropy Generation in Nanofluid's Axisymmetric Stagnation Flow over a Cylinder with Constant Wall Temperature and Uniform Surface Suction-Blowing, *Alexandria Eng. J.*, **54(4)**: 1483-1498 (2019).

[45] Zahmatkesh R., Mohammadiun H., Mohammadiun M., Dibaei Bonab M.H., Sadi M., Theoretical Investigation of Entropy Generation in Axisymmetric Stagnation Point Flow of Nanofluid Impinging on the Cylinder Axes with Constant Wall Heat Flux and Uniform Surface Suction-Blowing, *Iran. J. Chem. Chem. Eng. (IJCCE)*, **40(6):** 1893-1908 (2021).

[46] Hong L., Wang C.Y., Annular Axisymmetric Stagnation Flow on a Moving Cylinder, *Int. J. Eng. Sci.*, **47(1)**: 141–152 (2009).

[47] Wang C.Y., Off-Centered Stagnation Flow Towards a Rotating Disc, *Int. J. Eng. Sci.*, **46 (4)**: 391–396 (2008).

[48] Song D., Hatami M., Wang Y., Jing D., Yang Y., Prediction of Hydrodynamic and Optical Properties of TiO_2/Water Suspension Considering Particle Size Distribution, *Int. J. Heat Mass Trans.*, **92**: 864–876 (2016).

[49] Hatami M., Song D., Jing D., Optimization of a Circular-Wavy Cavity Filled by Nanofluid under the Natural Convection Heat Transfer Condition, *Int. J. Heat Mass Trans.*, **98**: 758–767(2016).

[50] Hatami M., Safari H., Effect of Inside Heated Cylinder on the Natural Convection Heat Transfer of Nanofluids in a Wavy-Wall Enclosure, *Int. J. Heat Mass Trans.*,**103**: 1053–1057(2016).

[51] Mosayebidorcheh S., Hatami M., Analytical Investigation of Peristaltic Nanofluid Flow and Heat Transfer in an Asymmetric Wavy Wall Channel (Part I: Straight Channel), *Int. J. Heat Mass Trans.*,**126**: 790–799(2018).

[52]Hatami M., Sheikholeslami M., Domairry D., High Accuracy Analysis for Motion of a Spherical Particle in Plane Couette Fluid Flow by Multi-Step Differential Transformation Method, *Powder Technol.*,**260**: 59–67(2014).

[53] Ghasemi S.E., Vatani M., Hatami M., Gangi D.D., Analytical and Numerical Investigation of Nanoparticle Effect on Peristaltic Fluid flow in Drug Delivery Systems, *J. Mol. Liq.*, **215**: 88–97(2016).

[54] Hatami M., Numerical Study of Nanofluids Natural Convection in a Rectangular Cavity Including Heated Fins, *J. Mol. Liq.*, **233**: 1–8 (2017).

[55]Hatami M., Nanoparticles Migration Around the Heated Cylinder During the RSM Optimization of a Wavy-Wall Enclosure, *Adv. Powder Technol.*, **28(3)**: 890–899 (2017).

[56] Ali K., Ahmad S., Baluch O., Jamshed W., Eid M.R., Pasha A.A., Numerical Study of Magnetic Field Interaction with Fully Developed Flow in a Vertical Duct, *Alexandria Eng. J.*, **61(12)**: 11351–11363(2022).

[57] Hatami M., Ganji D.D., Motion of a spherical Particle In a Fluid Forced Vortex by DQM and DTM, *Particuology.*, **16**: 206–212 (2014).

[58] Pourmehran O., Gorji M.R., Hatami M., Sahebi S.A.R., Domairry G., Numerical Optimization of Microchannel Heat Sink (MCHS) Performance Cooled by KKL Based Nanofluids in Saturated Porous Medium, *J. Taiwan Inst. Chem. Eng.*, **55**: 49–68 (2015).

[59] Ahmad S., Akhter S., Shahid M. I., Ali K., Akhtar M., Ashraf M., Novel Thermal Aspects of Hybrid Nanofluid Flow Comprising of Manganese Zinc Ferrite $MnZnFe_2O_4$, Nickel Zinc Ferrite $NiZnFe_2O_4$ and Motile Microorganisms, *Ain Shams Engineering Journal.*, **13 (5)**: 101668 (2022).

[60] Ahmad S., Younis J., Ali K., Rizwan M., Ashraf M., Abd el Salam M A., Impact of Swimming Gyrotactic Microorganisms and Viscous Dissipation on Nanoparticles Flow through a Permeable Medium: A Numerical Assessment, *J. Nanomater.*, **2022**:.

[61] Ahmad S., Ali K., Haider T., Jamshed W., Tag El Din E.S.M., Hussain S.M., Thermal Characteristics of Kerosene Oil-Based Hybrid Nanofluids (Ag-$MnZnFe_2O_4$): A Comprehensive Study, *Frontiers in Energy Research.*, **10**: (2022).

[62] Ali K., Ahmad A., Ahmad S., Ahmad S., Jamshed W., A Numerical Approach for Analyzing the Electromagnetohydrodynamic Flow Through a Rotating Microchannel, *Arabian J. Sci. Eng.*, (2022).

[63] Ali K., Ahmad S., Ahmad S., Jamshed W., Hussain S. M., Tag El Din E.S.M., Molecular Interaction and Magnetic Dipole Effects on Fully Developed Nanofluid Flowing *via* a Vertical Duct Applying Finite Volume Methodology, *Symmetry*, (2022).

[64]Aghayari R., Maddah H., Arani J.B., Mohammadiun H., Nikpanje E., An Experimental Investigation of Heat Transfer of Fe_2O_3/Water Nanofluid in a Double Pipe Heat Exchanger, *Int. J. Nano Dimens.* **6(5):** 517-524(2015).

[65]Aghayari R., Maddah H.,Faramarzi A.R., Mohammadiun H., Mohammadiun M., Comparison of the Experimental and Predicted Data for Thermal Conductivity of Iron Oxide Nanofluid Using Artificial Neural Networks, *Nanomed. Res. J.*, **1(1)**: 15-22 (2016).

[66] Habibi M.R., Amini M., Arefmanesh A., Ghasemikafrudi E., Effects of Viscosity Variations on Buoyancy-Driven Flow from a Horizontal Circular Cylinder Immersed in Al_2O_3-Water Nanofluid, *Iran. J. Chem. Chem. Eng., (IJCCE)*, **38 (1)**: 213-232 (2019).

[67] Nematollahzadeh A., Jangara H., Exact Analytical and Numerical Solutions for Convective Heat Transfer in a Semi-Spherical Extended Surface with Regular Singular Points, *Iran. J. Chem. Chem. Eng. (IJCCE)*, **40 (3)**: 980-989 (2021).

[68] Ozicik M.N., Orlande H.R.B., "Inverse Heat Transfer Fundamentals and Application", Taylor & Francis, New York, (2000).

[69] Azimi A., "Thermo-Hydraulically Simulation of Thermal Systems Using Inverse Evaluation", Ph.D. Thesis, Sharif University of Technology, Tehran, Iran. (2007).

[70] Beck J.V., Arnold K.J., "Parameter Estimation in Engineering and Science", John Wiley & Sons Inc., New York, (1977).

[71] Montazeri M., Mohammadiun H., Mohammadiun M., Dibaee Bonab M.H., Inverse Estimation of Time-Dependent Heat flux in Stagnation Region of Annular Jet on a Cylinder Using Levenberg-Marquardt Method, *Iran. J. Chem. Chem. Eng. (IJCCE)*, **41 (3)**: 971-988 (2022).